Cancer Nanotechnology

RESEARCH Open Access

Aptamer modified Ti_3C_2 nanosheets application in smart targeted photothermal therapy for cancer

Zhiqiang Bai[1,2], Lu Zhao[2], Haidi Feng[2], Zhihui Xin[1,2], Chaoyu Wang[2], Zhixiong Liu[2], Maozhong Tian[2], Haifei Zhang[4], Yunfeng Bai[2*] and Feng Feng[1,2,3*]

*Correspondence: baiyunfeng1130@126.com; feng-feng64@263.net

[1] School of Chemistry and Material Science, Shanxi Normal University, Linfen 041004, People's Republic of China
[2] School of Chemistry and Chemical Engineering, Shanxi Provincial Key Laboratory of Chemical Biosensing, Shanxi Datong University, Datong 037009, People's Republic of China
[3] Department of Energy Chemistry and Material Engineering, Shanxi Institute of Energy, Taiyuan 030600, People's Republic of China
[4] Department of Chemistry, University of Liverpool, Crown Street, Liverpool L69 7ZD, UK

Abstract

Background: Ti_3C_2 is a type of transition metal carbides and nitrides (MXenes) with high light-to-heat conversion efficiency property, which has been widely used in cancer treatment recently. In fact, active targeting delivery of MXenes nanomaterials with targeting molecule could enhance the therapeutic efficacy. However, targeted therapy of MXenes has not been further studied in the past. Aptamers (Apt) with excellent affinity and high specificity properties have been widely used as targeting tools. Predictably, the incorporation of Apt into Ti_3C_2 nanomaterials will offer an unprecedented opportunity in the research fields of cancer targeted therapy.

Results: Transmembrane glycoprotein mucin 1 (MUC1) is overexpressed on the surface of MCF-7 cells, and MUC1 Apt (Apt-M) could target MCF-7 cells with high affinity and specificity. Here, a smart targeting nanotherapeutic system Ti_3C_2/Apt-M was fabricated, which could specifically recognize and enter in MCF-7 cells. Benefitting from the desirable targeted performance of Apt-M, MCF-7 cells completed the ingestion process of Ti_3C_2/Apt-Mf nanosheets within 4 h, and Apt-M facilitated the entry of the Ti_3C_2/Apt-Mf nanosheets into MCF-7 cells. Besides, Ti_3C_2/Apt-M nanosheets exhibited the potential as an outstanding photothermal agent (PTA) because of the photothermal performance inherited from wrapped Ti_3C_2 nanosheets. As demonstrated, upon 808 nm laser irradiation, the Ti_3C_2/Apt-M nanotherapeutic system displayed a satisfactory antitumor effect by targeted photothermal therapy both in vitro and in vivo.

Conclusion: This study provides a new idea for the development of MXenes nanotherapeutic system with high active targeting performance.

Keywords: Ti_3C_2, Photothermal therapy, Aptamer, Targeted, Cancer

Graphical Abstract

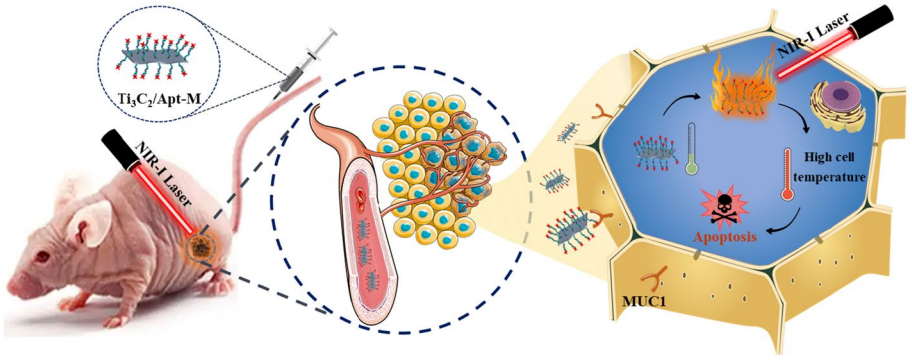

Introduction

Targeted delivery of anticancer drugs or nanomaterials to enhance therapeutic efficacy has become a new trend in cancer treatment (Zhu et al. 2022). Active cancer targeting can be achieved by conjugating different tissue-specific groups or ligands to nanomaterials surface, including peptides, antibodies, small molecules, aptamers (Apt) and so on (Arslan et al. 2021; Tan et al. 2021). Particularly, Apt is a class of artificially synthesized short- and single-stranded DNA or RNA sequences, which has a broad range of targets, including small molecules, peptides, proteins, cells and even viruses (Li et al. 2021). Apt have been widely used as promising targeting moieties, which due to their significant advantages, including high selectivity and affinity, high thermal stability, low toxicity and immunogenicity, low molecular weight, easy synthesis and modification (Xie et al. 2021). Such significant advantages make Apt a suitable alternative for peptides, antibodies, small molecules (Liu et al. 2022a; Yuhan et al. 2022). As a result, Apt have to be used as targeting tools for various anticancer drugs or nanomaterials delivery, such as Au nanocage (Yang et al. 2021), carbon spheres (Sargazi et al. 2022), graphene oxide (Du et al. 2020), mesoporous silica (Vandghanooni et al. 2020), MOF (Alijani et al. 2020), and DNA origami (Pan et al. 2020).

Two-dimensional (2D) titanium carbide (Ti_3C_2) nanomaterial is a kind of transition metal carbides and nitrides (MXenes), which was first synthesized by etching Ti_3AlC_2 with HF acid in 2011 (Li et al. 2019; Naguib et al. 2011; VahidMohammadi et al. 2021). To date, nearly 30 types of MXenes have been successfully experimentally synthesized, however, more than 100 types of MXenes have been computationally predicted (Gogotsi and Anasori 2019). Ti_3C_2 nanomaterial was gifted with some exciting and unique properties such as high surface-to-volume ratio, high atomic number, paramagnetic behavior and high light-to-heat conversion efficiency properties, which make it especially suitable nanoplatform for the application of tumor therapy (Huang et al. 2022; Xu et al. 2022; Wu et al. 2022; Han et al. 2018; Tang et al. 2019). With the passively targeted and accumulated in tumor tissues through enhanced permeability and retention (EPR) effects, Ti_3C_2 nanomaterial could be used as cancer treatment and theranostics applications (Lin et al. 2017; Liang et al. 2019; He et al. 2022; Li

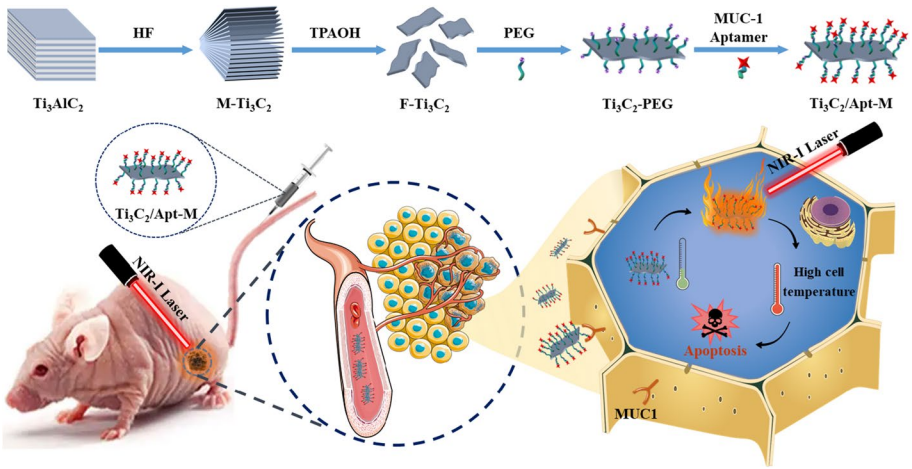

Scheme 1 Schematic illustration of Ti_3C_2/Apt-M nanotherapeutic system for smart targeted photothermal therapy for cancer

et al. 2022; Zhang et al. 2022). However, active targeting delivery of Ti_3C_2 nanomaterial could enhance the accumulation of nanomaterials at tumor sites and improve the effect of tumor treatment (Liu et al. 2020, 2017, 2021; Li et al. 2018).

Transmembrane glycoprotein mucin 1 (MUC1) was a heterodimeric protein overexpressed on the surface of tumor cells in most malignant tumors including breast, ovarian and lung cancers (Correa et al. 2022). Moreover, MUC1 aptamer (Apt-M) has been developed to target MUC1-expressing cancer cells such as MCF-7 with high affinity and specificity, which could enhance anticancer nanomaterials delivery in cancer therapy (Khan et al. 1239).

Herein, a smart targeting nanotherapeutic system Ti_3C_2/Apt-M (Scheme 1) was developed for cancer-targeted photothermal therapy (PTT). In this work, the Apt-M was covalently bound to the surface of nanotherapeutic system, which enable MCF-7 cells ingest more Ti_3C_2/Apt-M nanosheets. As expected, the temperature of Ti_3C_2/Apt-M nanotherapeutic system raised rapidly under laser irradiation, which achieve the purpose of PTT. Furthermore, the Ti_3C_2/Apt-M nanotherapeutic system inhibited tumor growth using targeted PTT has been systematically demonstrated in vitro and in vivo. This study provides a new idea for the development of MXenes nanotherapeutic system with smart targeting performance.

Results and discussion

Synthesis and characterization

Ti_3C_2 nanosheets were prepared from bulk Ti_3AlC_2 by chemical exfoliation method (Lin et al. 2017). After HF etching to remove the Al layer, the prepared Ti_3C_2 bulk showed an accordion-like structure (Additional file 1: Fig. S1). After further intercalation with TPAOH, the prepared Ti_3C_2 nanosheets has an ultrathin 2D sheet-like morphology with excellent hydrophilicity and dispersibility (Fig. 1a). The theoretical thickness of Ti_3C_2 nanosheet is 0.474 nm (Lin et al. 2017). AFM profile showed the average lateral size of Ti_3C_2 nanosheet was about 100 nm and the thickness was lower than 1.74 nm, which proved that the prepared Ti_3C_2 nanosheets had fewer layers (Additional file 1: Fig. S2).

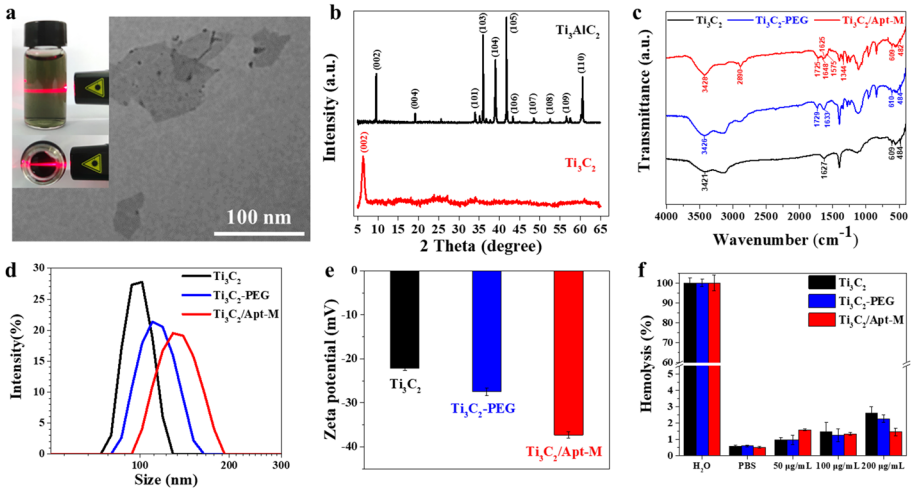

Fig. 1 Synthesis and characterization. (**a**) TEM image of Ti_3C_2 nanosheets (inset shows a digital photo of Ti_3C_2 nanosheets dispersed in water exhibiting Tyndall effect). (**b**) XRD patterns of Ti_3AlC_2 ceramic bulks and Ti_3C_2 nanosheets. (**c**) FT–IR spectra, (d) Dynamic light scattering analysis and (**e**) zeta potential analysis of Ti_3C_2, Ti_3C_2-PEG and Ti_3C_2/Apt-M nanosheets. (**f**) Hemolysis assay of Ti_3C_2, Ti_3C_2-PEG and Ti_3C_2/Apt-M nanosheets at different concentrations

The EDS (Additional file 1: Fig. S3) and XPS (Additional file 1: Fig. S4) results showed that the Al element was completely removed in the prepared Ti_3C_2 nanosheets (Additional file 1: Figs. S3, S4). XRD further revealed that only the (002) peak at 6.0° was still evident in Ti_3C_2 nanosheets (Fig. 1b). Taken together, these results proved that Ti_3C_2 nanosheets was successfully prepared.

After the surface modification of COOH–PEG–COOH, the stretching vibration of C=O in carboxyl group at ~ 1729 cm^{-1} was found in FT–IR spectra of Ti_3C_2-PEG (Fig. 1c) (Yathindranath et al. 2013). The $-NH_2$ modified Apt-M was immobilized on the surface of Ti_3C_2-PEG nanosheets by EDC-NHS reaction. FT–IR spectra of Ti_3C_2/Apt-M showed the characteristic absorption peak of amide bond at ~ 1648 cm^{-1} (amide peak I, stretching vibration of C=O), ~ 1575 cm^{-1} (amide peak II, bending vibration of N–H) and ~ 1344 cm^{-1} (amide peak III, stretching vibration of C–N) (Du et al. 2020). In addition, the hydrodynamic diameter of Ti_3C_2/Apt-M (139 nm) increased slightly compared with those of Ti_3C_2-PEG (119 nm) and Ti_3C_2 (101 nm) (Fig. 1d). Moreover, the zeta potential of Ti_3C_2, Ti_3C_2-PEG and Ti_3C_2/Apt-M was measured as −22.10, −27.43 and −37.30 mV, respectively (Fig. 1e). These results indicated the successful PEG modification and Apt-M functionalization.

The Ti_3C_2/Apt-M nanosheets showed excellent stability and dispersibility in various physiological media (Additional file 1: Fig. S5). Furthermore, the Ti_3C_2/Apt-M nanosheets didn't cause significant hemolysis (< 5%) even at a high concentration of 200 μg mL^{-1} (Fig. 1f, Additional file 1: Fig. S6) (Chang et al. 2022). Interestingly, the UV–vis absorption of Ti_3C_2/Apt-M at 808 nm did not change significantly compared to Ti_3C_2 (Additional file 1: Fig. S7).

Photothermal performance

To assess the photothermal performance of Ti_3C_2/Apt-M nanosheets, the extinction coefficient (α) was evaluated to be 16.9 Lg^{-1} cm^{-1} according to Lambert–Beer law (Fig. 2a), which was superior to other Ti_3C_2 MXenes composite nanosheets, such as Ti_3C_2-IONP@PEG-GOD nanoparticle (8.57 Lg^{-1} cm^{-1}) (Liang et al. 2019) and Ti_3C_2-PEG-OVA-Mn^{2+} nanoparticle (6.40 Lg^{-1} cm^{-1}) (Liu et al. 2022b). Furthermore, the photothermal conversion efficiency (η) of Ti_3C_2/Apt-M nanosheet was calculated to be as high as 31.76% (Fig. 2b, c), which was significantly higher than that of Ti_3C_2-IONP@PEG-GOD nanoparticle (27.27%) (Liang et al. 2019) and Ti_3C_2-PEG-OVA-Mn^{2+} nanoparticle (28.17%) (Liu et al. 2022b). The temperature of Ti_3C_2/Apt-M solutions raised with the increase of Ti_3C_2/Apt-M concentration and laser power density, suggesting the photothermal properties of the Ti_3C_2/Apt-M nanosheets were concentration dependent (Fig. 2d, e) and power dependent (Additional file 1: Fig. S10). It was noteworthy that the temperature of the Ti_3C_2/Apt-M nanosheets (100 μg mL^{-1}) could reach 67.6 °C under 808 nm irradiation in 10 min, which was enough for photothermal tumor ablation (Lu et al. 2022). Moreover, Ti_3C_2/Apt-M nanosheets exhibited satisfactory photothermal stability in five laser on/off cycles (Fig. 2f).

Intracellular endocytosis and targeting performance analysis

The affinity and specificity of Apt-M with cancer cells were verified by flow cytometry. A significant increase of fluorescence intensity from Apt-Mf in MCF-7 cells was observed, which was significantly stronger than that of the MCF-7 cells incubated with Apt-Cf

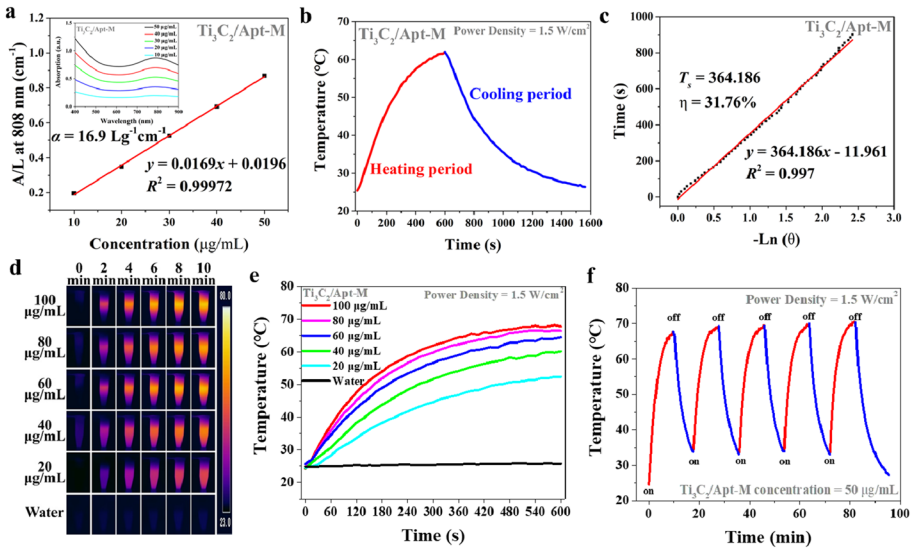

Fig. 2 The photothermal performance of Ti_3C_2/Apt-M nanosheets. **a** Mass extinction coefficient of Ti_3C_2/Apt-M nanosheets at 808 nm (inset shows UV–vis spectra of Ti_3C_2/Apt-M nanosheets at different concentrations). **b** Photothermal performance of Ti_3C_2/Apt-M nanosheets dispersed in aqueous solution under 808 nm laser irradiation. **c** Calculation of time constant and photothermal-conversion efficiency of Ti_3C_2/Apt-M nanosheets at 808 nm laser irradiation. **d** Infrared thermal images and **e** temperature changes of Ti_3C_2/Apt-M nanosheet aqueous solutions with different concentrations (20, 40, 60, 80 and 100 μg mL^{-1}) under 808 nm laser irradiation. **f** Temperature curve of Ti_3C_2/Apt-M nanosheet aqueous solution under five 808 nm laser on/off cycles

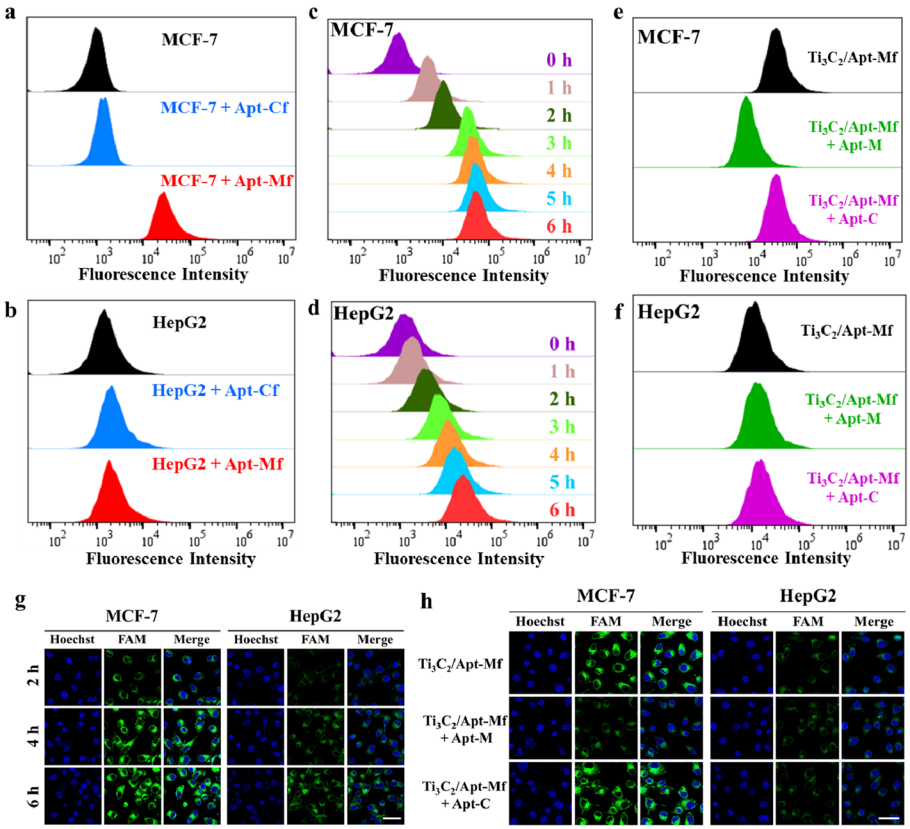

Fig. 3 Active targeting performance analysis of Ti_3C_2/Apt-M nanosheets. Flow cytometry analysis of **a** MCF-7 and **b** HepG2 cells after incubation with Apt-Cf or Apt-Mf. Flow cytometric analysis of (**c**) MCF-7 and (d) HepG2 cells incubated with Ti_3C_2/Apt-Mf nanosheets for different time (0, 1, 2, 3, 4, 5 and 6 h). Flow cytometric analysis of **e** MCF-7 and **f** HepG2 cells incubated with Ti_3C_2/Apt-Mf, Ti_3C_2/Apt-Mf with free Apt-C, Ti_3C_2/Apt-Mf with free Apt-M for 4 h. **g** CLSM images of MCF-7 and HepG2 cells incubated with Ti_3C_2/Apt-Mf for 2, 4 and 6 h. Scale bar: 50 μm. **h** CLSM images of MCF-7 and HepG2 cells incubated with Ti_3C_2/Apt-Mf, Ti_3C_2/Apt-Mf with free Apt-M, Ti_3C_2/Apt-Mf with free Apt-C for 4 h. Scale bar: 50 μm

(Fig. 3a). Meanwhile, no obvious change was observed in HepG2 cells when incubated with Apt-Mf or Apt-Cf, implying that Apt-M had specificity to MCF-7 cells (Fig. 3b).

To reveal the smart targeting performance of Ti_3C_2/Apt-M nanosheets, flow cytometry was used to verify the fluorescence intensity of MCF-7 or HepG2 cells after incubation with Ti_3C_2/Apt-Mf for different time. The fluorescence intensity of MCF-7 cells was significantly higher than that of HepG2 cells at the same time (Fig. 3c, d). Moreover, the fluorescence intensity of MCF-7 cells was not significantly increased after 4 h. The results indicated that MCF-7 cells completed the ingestion process of Ti_3C_2/Apt-Mf nanosheets within 4 h, and Apt-M facilitated the entry of the Ti_3C_2/Apt-Mf nanosheets into MCF-7 cells. For competitive study, MCF-7 cells were pre-incubated with free Apt-M or Apt-C. As expected, the fluorescence intensity of MCF-7 cells was significantly decreased after pre-incubated with free Apt-M (Fig. 3e). Meanwhile, negligible changes in fluorescence intensity were observed in HepG2 cells after pre-incubation with free Apt-C or Apt-M, indicating the ingestion of Ti_3C_2/Apt-M nanosheets into cells was mediated by Apt-M (Fig. 3f). Furthermore, CLSM was conducted to

investigate the ingestion behavior and targeting efficacy of Ti_3C_2/Apt-M nanosheets, and the results indicated that the ingestion of Ti_3C_2/Apt-M nanosheets into cells was mediated by Apt-M, which in accordance with the flow cytometry results (Fig. 3g, h).

In vitro targeted photothermal therapy against tumor cell growth

The in vitro anticancer performances of Ti_3C_2/Apt-M nanosheets were evaluated by MTT assay. Negligible toxicity on the MCF-7 and HepG2 was observed after 24 or 48 h treatment with Ti_3C_2-PEG, Ti_3C_2/Apt-C or Ti_3C_2/Apt-M nanosheets, even at a high concentration of 400 μg mL^{-1} (Additional file 1: Fig. S11). Furthermore, the targeted photothermal therapy against cell growth was assessed under 808 nm laser irradiation. The results showed that only 43.1% of MCF-7 cells survived in Ti_3C_2-PEG + Laser group (Fig. 4a). With the aid of the excellent targeting ability of Apt-M, the viability of MCF-7 cell treated with Ti_3C_2/Apt-M + laser was only 22.7% under the smart-targeted PTT. It was notable that the HepG2 cell viabilities of Ti_3C_2/Apt-M + Laser group were not significantly different from that of Ti_3C_2-PEG + Laser group. Furthermore, compared with Ti_3C_2-PEG and Ti_3C_2/Apt-C, Ti_3C_2/Apt-M nanosheets showed excellent targeted therapeutic effects on MCF-7 at different concentrations (Additional file 1: Fig. S12). The MTT results further confirmed the targeted therapeutic effect of Ti_3C_2/Apt-M nanosheets were mediated by Apt-M, which making them more ingested by MCF-7 cells and displayed a concentration-dependent anticancer performance.

Additionally, to reveal the desirable targeted PTT effect by Ti_3C_2/Apt-M, cells after treatments were stained with Calcein-AM and PI, respectively, and observed

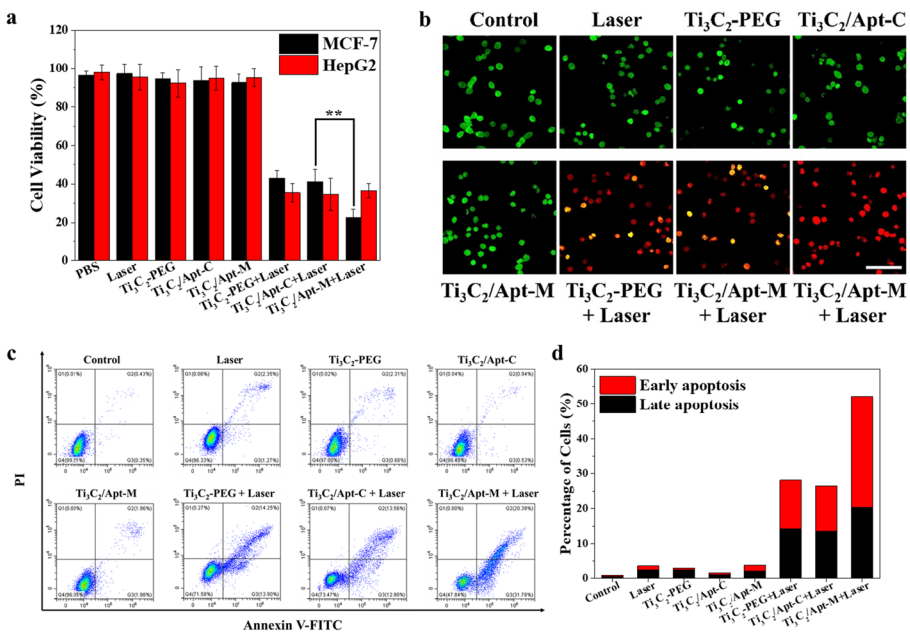

Fig. 4 In vitro targeted photothermal therapy against tumor growth. **a** Cell viability of MCF-7 and HepG2 cells after 4 h incubation with different nanomaterials and treatments. **b** CLSM images of MCF-7 cells stained with Calcein-AM (green fluorescence) and PI (red fluorescence) staining. Scale bar: 100 μm. **c** Flow cytometry apoptosis analysis of Annexin V-FITC and PI strained MCF-7 cells. **d** Quantification analysis of the percentages of apoptotic cells after various treatments in flow cytometry

by CLSM. Ti_3C_2/Apt-M could effectively ablate the MCF-7 cells under laser irradiation as evidenced by the number of dead cells with red fluorescence (PI), which was in consistent with the MTT results (Fig. 4b). The targeted PTT against MCF-7 cell was further investigated by flow cytometry analysis. The percentage of apoptotic cells (including early and late apoptotic cells) induced by Ti_3C_2/Apt-M + Laser reached 52.17%, which exhibited the highest therapeutic efficacy among all treatments (Fig. 4c–d).

In vivo-targeted photothermal therapy against tumor growth

Motivated by the desirable in vitro-targeted PTT performance, the MCF-7 cell xenograft mice models were established and used for the targeted PTT in vivo. As expected, the surface temperature of tumor sites in Ti_3C_2/Apt-M + Laser treatment mice increased rapidly to 61.4 °C, which was significantly higher than other laser irradiated groups, suggesting that the Ti_3C_2/Apt-M nanosheets could smartly target MCF-7 cells and increase the accumulation in tumor areas (Additional file 1: Fig. S13). The body weight fluctuations of all mice were negligible during the treatment period (Additional file 1: Fig. S14), indicating the satisfactory biosafety of the Ti_3C_2/Apt-M nanosheets in vivo treatment. More importantly, the tumor volume of mice treated with Ti_3C_2/Apt-M + Laser was suppressed effectively, while the tumors in other treatment groups continuously grew at similar rates (Fig. 5a–c). Moreover, the tumor weight in Ti_3C_2/Apt-M + Laser treatment group was significantly lower than other treatment groups (Fig. 5d). The results strongly suggested that Apt-M mediated targeted PTT display excellent therapeutic effect for suppressing the tumor growth, although the photothermal conversion efficiency of

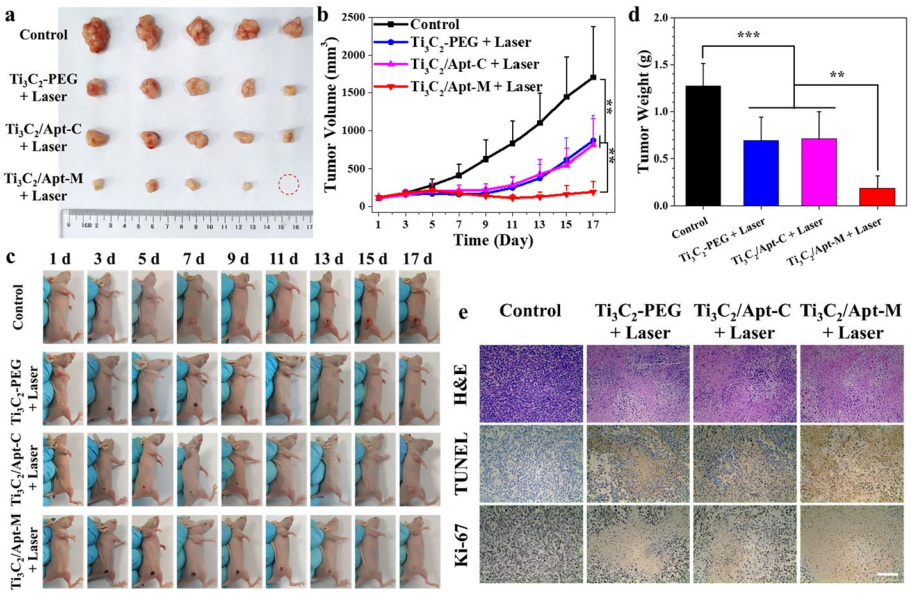

Fig. 5 In vivo targeted photothermal therapy against tumor growth. **a** Digital photos of excised tumors from sacrificed mice at the end of therapy. **b** Time-dependent tumor volume curves of tumor-bearing mice after different treatments in 17 d. **c** Representative digital photographs of tumor-bearing mice after different treatments. **d** Tumor weight of excised tumors from sacrificed mice at the end of therapy. **e** H&E staining, TUNEL staining and Ki-67 staining of excised tumor tissue after different treatments. Scale bar: 100 μm

Ti_3C_2/Apt-M nanosheets is not the most prominent among MXenes and other inorganic photothermal agents (Additional file 1: Table S2).

Furthermore, the tumors were harvested and stained by hematoxylin–eosin (H&E) and immunohistochemistry (IHC). For H&E staining, Ti_3C_2/Apt-M + Laser treatment group showed obvious tumor tissue shrinkage and damage compared to the other groups (Fig. 5e). TDT-mediated dUTP nick-end labelling (TUNEL) IHC staining was taken to further reveal the apoptosis of tumor cells, and the high expression of this marker was shown in the tumor from mice treated with Ti_3C_2/Apt-M + Laser. Similarly, Ki-67 IHC staining results verified the least cell proliferation with the treatment of Ti_3C_2/Apt-M + Laser in tumor tissues compared with other groups, while further demonstrating the better targeted therapeutic effect on inhibiting the tumor growth. Moreover, to investigate the biosafety of the proposed targeted PTT, the major organs (heart, liver, spleen, lung, and kidney) were gathered and sectioned for H&E staining and any toxic effects or inflammation could not be observed in these organs (Fig. S15). Overall, Ti_3C_2/Apt-M was a highly promising targeted photothermal agent (PTA) for in vivo tumor targeted therapy with satisfactory biosafety.

Conclusions

In summary, this work successfully designed a distinctive Ti_3C_2/Apt-M nanosheets for smart-targeted photothermal therapy of cancer in vitro and in vivo. Especially, the Ti_3C_2 nanosheets covalently linked Apt-M were endowed with smart targeting properties, which could specifically recognize and enter in MCF-7 cells. Moreover, Ti_3C_2/Apt-M nanosheets exhibited the potential as an outstanding PTA because of the photothermal performance inherited from wrapped Ti_3C_2 nanosheets. As demonstrated, upon 808 nm laser irradiation, the Ti_3C_2/Apt-M nanosheets displayed a satisfactory antitumor effect by targeted photothermal therapy both in vitro and in vivo. This work expanded the application of MXenes for targeted therapy. More commendable, different types of Apt could be used for different types of tumors, so as to achieve precision medicine and personalized medicine.

Experimental

Materials

Ti_3AlC_2 (> 98%, 200-meshes) ceramics powder was purchased from Shanghai Mclean Biochemical Technology Co., Ltd. Hydrofluoric acid (HF, AR, 40.0%), tetrapropylammonium hydroxide (TPAOH, AR, 40.0%) and Dimethyl Sulfoxide (DMSO) were obtained from Shanghai Adamas reagent Co., Ltd. The COOH-PEG-COOH (MW 4000) was purchased from Shanghai Yare Biotechnology Co., Ltd. 1-Ethyl-3-(3-dimethylaminopropyl) carbodiimide Hydrochloride (EDC•HCl) and N-Hydroxysuccinimide (NHS) were acquired from Shanghai Aladdin reagent Co., Ltd. The phosphate buffered saline (PBS), trypsin, 3-(4,5-Dimethylthiazol-2-yl)-2,5-diphenyltetrazolium bromide (MTT) and penicillin/streptomycin were obtained from Shanghai Sigma–Aldrich Trading Co., Ltd. Fetal Bovine Serum (FBS) were obtained from Biological Industries reagent Co., Ltd. The Roswell Park Memorial Institute-1640 (RPMI-1640) medium was purchased from Biosharp reagent Co. Hoechst 33342 reagent, Calcein AM/PI cytotoxicity assay kit

and Annexin V-FITC/PI apoptosis assay kit were purchased from Shanghai Beyotime Biotechnology Co., Ltd. MUC1 Apt (Apt-M), control Apt (Apt-C), 5-Carboxyfluorescein (FAM) labeled Apt-M (Apt-Mf) and FAM-labeled control Apt (Apt-Cf) sequences (Additional file 1: Table S1) were synthesized and HPLC purified by Shanghai Sangon Biotech Co., Ltd.

Characterizations

Scanning Electron Microscope (SEM) images were measured by TESCAN MAIA3 microscope. Transmission Electron Microscope (TEM) images were obtained by JEOL JEM-2100F transmission electron microscope at 200 kV accelerating voltage, and the elements composition of Ti_3C_2 nanosheets was analyzed by X-MaxN 80 T IE250 energy dispersive spectroscopy (EDS). Atomic Force Microscope (AFM) measurement was carried out on Bruker Dimension Icon system at typical rate of 3 min per image. X-ray diffraction (XRD) patterns were recorded on a Rigaku SmartLab SE diffractometer, with the angles from 5° to 65° and the rate of 2° min^{-1}. X-ray photoelectron spectroscopy (XPS) spectra was detected by a Thermo Scientific K-Alpha XPS energy spectrometer. Fourier transform infrared (FT–IR) spectra were recorded by a Thermo Scientific NICOLET iS20 Spectrometer. Hydrodynamic size and zeta potentials of nanomaterials were measured using Malvern Zetasizer Nano ZS90 nano particle potential meters. PerkinElmer Lambda35 spectrometer was used to record UV–vis absorption spectra. The laser irradiation was conducted by a high-power 808 nm multimode pump (Cnilaser DPS–808–Q) laser of Changchun new industry photoelectric technology Co., Ltd. The temperature and thermal images were recorded on an FOTRIC 323pro infrared thermal imager. The absorbance value of 96-well plate was measured by Tecan Infinite M200PRO microplate reader. Beckman Coulter CytoFLEX flow cytometer was used for the flow cytometry experiments. The confocal laser scanning microscopy (CLSM) images were recorded using an Olympus FV1200V inverted CLSM.

Preparation of Ti_3C_2 nanosheets (MXenes)

Ti_3C_2 nanosheets were prepared from Ti_3AlC_2 by chemical exfoliation method (Lin et al. 2017). In brief, Ti_3AlC_2 ceramics (1.0 g) were slowly suspended in 20 mL of a 40% HF aqueous solution (Please take personal protection when using this hazards reagent), stirred at room temperature for 3 d. Then, the precipitate was washed with deionized water and dispersed in 20 mL TPAOH aqueous solution (25 wt.%), stirred for 3 d at room temperature. Afterwards, the sediment was collected by centrifugation (3500 rpm, 10 min) and washed with deionized water for 6–8 times to make the pH of the solution greater than 6.0. The Ti_3C_2 was prepared after centrifugation at 3500 rpm for 60 min.

Preparation of Ti_3C_2-PEG and Ti_3C_2/Apt nanosheets

To attach COOH-PEG-COOH on the surface of Ti_3C_2 nanosheets, the 2.5 mL COOH–PEG–COOH (10.0 mg mL^{-1}) slowly dissolved in 2.5 mL Ti_3C_2

aqueous suspension (1.0 mg mL^{-1}) and stirred for 6 h at room temperature. Then, the Ti_3C_2-PEG nanosheets were obtained by centrifugation and washed three times with deionized water to remove excess COOH-PEG-COOH. Afterwards, 500 μL EDC•HCl (500 mM) and 500 μL NHS (100 mM) were slowly added to 1.0 mL Ti_3C_2-PEG nanosheets suspension (2.0 mg mL^{-1}) and stirred for 30 min at room temperature. The activated Ti_3C_2-PEG nanosheets were obtained by centrifugation and washed with deionized water for 3 times. Then, Apt was dispersed in the activated Ti_3C_2-PEG nanosheets and stirred for 6 h at room temperature. The Apt modified Ti_3C_2/Apt nanosheets were obtained by centrifugation and washed 3 times with deionized water to remove excess Apt.

Hemolysis assay

Erythrocytes were collected from mouse blood by centrifugation (3000 rpm, 3 min). Then, 4% erythrocytes (v/v, 1.0 mL) were incubated with PBS, H_2O, and different concentrations of nanosheets (1.0 mL, 50–200 μg mL^{-1}) at 37 °C for 8 h, respectively. After that, the supernatant was obtained by centrifugation (3000 rpm, 3 min) and its absorbance value was measured at 540 nm. The percentage of hemolysis can be measured from Eq. (1):

$$\text{Hemolysis}(\%) = \frac{A_1}{A_0} \times 100\% \tag{1}$$

where A_0 represents the absorbance of the supernatant after the erythrocytes were incubated with H_2O, and A_1 denotes the absorbance after incubated with other nanosheets solutions.

Photothermal performance of Ti_3C_2/Apt-M nanosheets

To evaluate the photothermal performance of Ti_3C_2/Apt-M nanosheets, these nanosheets with various concentrations (20, 40, 60, 80 and 100 μg mL^{-1}) were irradiated with the 808 nm laser at a power density of 1.5 W cm^{-2} for 10 min. Furthermore, the nanosheets irradiated with various power density (0.5, 1.0, 1.5, 2.0 and 2.5 W cm^{-2}) were also carried out. The temperature and thermal images were recorded by infrared thermal imager. The photothermal conversion efficiency (η) of Ti_3C_2/Apt-M was calculated according to Roper's report (Roper et al. 2007), as shown in Eq. (2):

$$\eta = \frac{hS\left(T_{max,NP} - T_{surr}\right) - Q_{dis}}{I\left(1 - 10^{-A_{808}}\right)} \tag{2}$$

where h is the heat transfer coefficient, S is the surface area of the container, T_{max} is the maximum temperature of the solution, T_{surr} is the surrounding temperature, I is the laser power density, and A_{808} is the absorption value of the material at 808 nm. Q_{dis} is the heat generated after water and container absorbs light. To calculate hS, Eq. (3, 4) was introduced:

$$Q_{dis} = hS(T_{max,H_2O} - T_{surr}) \tag{3}$$

$$\tau_s = \frac{m_D C_D}{hS} \tag{4}$$

m_D is the mass of water, C_D is the heat capacity of water (4.2 $J \cdot g^{-1} \cdot °C^{-1}$), τ_s is the sample system time constant, which was calculated by formula (5 , 6):

$$t = -\tau_s ln\theta \tag{5}$$

$$\theta = \frac{T_{surr} - T}{T_{surr} - T_{max}} \tag{6}$$

According to the obtained data and Eq. (2), the photothermal conversion efficiency of the Ti_3C_2, Ti_3C_2-PEG, Ti_3C_2/Apt-C and Ti_3C_2/Apt-M nanosheets was determined to be 36.72%, 33.25%, 32.19% and 31.76%, respectively.

The photothermal stability of Ti_3C_2/Apt-M was evaluated by five repeated laser on/off irradiations.

Affinity analysis between Apt and cells

MCF-7 and HepG2 cells were donated by Hunan University. MCF-7 and HepG2 cell line were cultured in RPMI-1640 with 10% FBS and 1% penicillin/streptomycin at 37 °C in a humidified incubator containing 5% CO_2. Then, the cells were collected and washed with PBS 2–3 times. Subsequently, the cells were blown to form a cell suspension and incubated with Apt-Mf or Apt-Cf for 2 h, respectively. Finally, the fluorescence intensity of the cells was evaluated by flow cytometry after the cells were washed and resuspended in 500 μL PBS.

Intracellular endocytosis analysis

For the intracellular endocytosis analysis, cells were seeded in 6-well plates (1×10^5 cells/well) for 24 h, and co-incubated with Ti_3C_2/Apt-Mf nanosheets (75 μg mL^{-1}) for 0, 1, 2, 3, 4, 5 and 6 h, respectively. The flow cytometry analysis was conducted after cells were gently washed three times with PBS.

In addition, cells were incubated in a CLSM culture dish at a density of 2×10^5 cells/dish for 24 h. After that, 75 μg mL^{-1} of Ti_3C_2/Apt-Mf nanosheets were added into the dish and co-incubated with the cells for 2, 4 and 6 h. The cells were washed with PBS gently. Afterwards, the cells were stained with Hoechst 33342 and observed by CLSM.

Targeting performance analysis

The targeting performance was analyzed by flow cytometry and CLSM. The cells were seeded in CLSM culture dish (2×10^5 cells/dish) or 6-well plates (2×10^5 cells/well) for 24 h. After that, the original medium was replaced with fresh medium containing Ti_3C_2/Apt-Mf (75 μg mL^{-1}), Ti_3C_2/Apt-Mf (75 μg mL^{-1}) + 2 OD Apt-M, Ti_3C_2/Apt-Mf (75 μg mL^{-1}) + 2 OD Apt-C, respectively. Then, the cells were analyzed by flow cytometry or CLSM after cultured for 4 h.

In vitro cytotoxicity assay

The cytotoxicity of Ti_3C_2-PEG, Ti_3C_2/Apt-C and Ti_3C_2/Apt-M nanosheets was evaluated by the standard MTT method. The cells were seeded into 96-well plates at 5×10^3 cells/well for 24 h. Then, different concentrations (0, 25, 50, 100, 200 and 400 μg mL^{-1}) of samples were added and incubated with cells for another 24 or 48 h. Afterwards, the culture medium was removed and cells were washed three times with PBS (200 μL). After that, the cell viabilities were detected by the MTT assay. The absorbance at 570 nm was measured on a microplate reader.

In vitro-targeted antitumor effect

Cells were seeded into 96-well plates at 5×10^3 cells/well for 24 h. Then, cells were incubated with PBS, Ti_3C_2-PEG (75 μg mL^{-1}), Ti_3C_2/Apt-C (75 μg mL^{-1}) and Ti_3C_2/Apt-M (75 μg mL^{-1}) for 4 h. Afterwards, cells were washed with PBS three times and then irradiated with 808 nm laser at a power density of 1.5 W/cm^2 for 10 min. Then, the cell viability was detected by MTT method after the cells were cultured for another 12 h.

Live/dead cells staining was used to visualize the targeted antitumor effect in vitro. After incubated with different groups of nanomaterial and irradiated with 808 nm laser, the cells were washed with PBS several times and stained by Calcein-AM and PI solution according to the manufacturer's protocol. Then, the CLSM was used to record the fluorescence images of living cells (green fluorescence) and dead cells (red fluorescence).

Furthermore, apoptosis analysis was performed to visualize the targeted antitumor effect. After incubated with different groups of nanomaterial and irradiated with 808 nm laser, cells were collected and stained by Annexin V-FITC and PI solution according to manufacturer's protocol. Then, flow cytometry was used to evaluate the cell signals after the cells were washed with PBS three times to remove redundant dyes.

In vivo targeted antitumor effect

Animal experiments were performed under the permission of experimental animal ethics committee of Shanxi Datong University. BALB/c nude mice were purchased from Beijing Huafukang Biotechnology Co., Ltd. The xenograft tumor model was established by injecting 5×10^6 cells of MCF-7 into the groin region of mice. The tumor volume was calculated and recorded according to the formula: tumor volume = (tumor length) × (tumor width)^2/2. When the tumor volume reached approximately 100 mm^3, all mice were randomly divided into four groups with five mice for each group, including: (1) Control group (PBS), (2) Ti_3C_2-PEG + Laser group (dose of Ti_3C_2-PEG = 15 mg kg^{-1}), (3) Ti_3C_2/Apt-C + Laser group (dose of Ti_3C_2/Apt-C = 15 mg kg^{-1}), (4) Ti_3C_2/Apt-M + Laser group (dose of Ti_3C_2/Apt-M = 15 mg kg^{-1}). All mice were injected intravenously with PBS, Ti_3C_2-PEG, Ti_3C_2/Apt-C or Ti_3C_2/Apt-M separately. After 4 h, the tumors of mice in groups (2), (3) and (4) were irradiated with 808 nm laser (1.5 W cm^{-2}) for 10 min. Afterwards, the body weight and tumor volume of mice were measured for continuous 17 d. Finally, all the dissected tumors were weighted up and collected for hematoxylin–eosin (H&E), terminal deoxynucleotidyl transferase dUTP nick

end labeling (TUNEL) and Antigen Ki-67 immunofluorescence staining. Additionally, the major organs including heart, lung, liver, spleen and kidney were obtained as well to make H&E-stained sections for observing whether these nanosheets could cause tissue damage.

Statistical analysis

Analysis of the data was conducted using SPSS version 21.0. The significance of the differences between the experiments and control groups was analyzed by one-way analysis of variance (ANOVA). Statistical significance was set at $^{*}P<0.05$, $^{**}P<0.01$ and $^{***}P<0.001$.

Supplementary Information

The online version contains supplementary material available at https://doi.org/10.1186/s12645-023-00189-4.

Additional file 1: Figure S1. SEM images of (a) Ti_3AlC_2 ceramic bulks and (b) Ti_3C_2 bulks. **Figure S2.** (a) AFM image and (b) the corresponding thickness of Ti_3C_2 nanosheets. **Figure S3.** EDS spectra of Ti_3C_2 nanosheets. **Figure S4.** XPS spectra of Ti_3C_2 nanosheets. **Figure S5.** Digital images of Ti_3C_2 nanosheets and Ti_3C_2/Apt-M nanosheets dispersed in various solvents. **Figure S6.** Digital images of hemolysis assay of Ti_3C_2, Ti_3C_2-PEG and Ti_3C_2/Apt-M nanosheets at different concentrations. **Figure S7.** UV–vis spectra of Ti_3C_2, Ti_3C_2-PEG and Ti_3C_2/Apt-M nanosheets. **Figure S8.** UV–vis spectra of (a) Ti_3C_2, (b) Ti_3C_2-PEG and (c) Ti_3C_2/Apt-C nanosheets at different concentrations. Mass extinction coefficient of (d) Ti_3C_2, (e) Ti_3C_2-PEG and (f) Ti_3C_2/Apt-C nanosheets at 808 nm. Normalized absorbance intensity at $\lambda = 808$ nm divided by the characteristic length of the cell (A/L) at varied concentrations (10, 20, 30, 40 and 50 μg mL^{-1}). **Figure S9.** Photothermal performance of (a) Ti_3C_2, (b) Ti_3C_2-PEG and (c) Ti_3C_2/Apt-C nanosheets dispersed in aqueous solution under 808 nm laser irradiation. Calculation of time constant and photothermal-conversion efficiency of (d) Ti_3C_2, (e) Ti_3C_2-PEG and (f) Ti_3C_2/Apt-C nanosheets at 808 nm laser irradiation. **Figure S10.** (a) Infrared thermal images and (b) temperature changes of Ti_3C_2/Apt-M nanosheet aqueous solutions under different laser power irradiation at 808 nm. **Figure S11.** Cell viabilities of (a-b) MCF-7 and (c-d) HepG2 cells after incubation with Ti_3C_2-PEG, Ti_3C_2/Apt-M and Ti_3C_2/Apt-C nanosheets of varied concentrations for 24 h and 48 h. **Figure S12.** Cell viability of (a) MCF-7 and (b) HepG2 cells treated with different concentrations of Ti_3C_2-PEG, Ti_3C_2/Apt-C and Ti_3C_2/Apt-M nanosheets. **Figure S13.** (a) The representative infrared thermal images and (b) temperature curves of tumor-bearing mice with different treatments at different time points. **Figure S14.** Body weight curves of tumor-bearing mice after different treatments in 17 d. **Figure S15.** H&E stained tissue sections of major organs (heart, liver, spleen, lung and kidney) from mice with different treatments. Scale bar: 100 μm. **Table S1.** Aptamer sequences. **Table S2.** The photothermal performance parameters (mass extinction coefficient and photothermal conversion efficiency) of various nanoagents in the literatures.

Acknowledgements

This research was sponsored by grants from Cultivate Scientific Research Excellence Programs of Higher Education Institutions in Shanxi (Grant No. 2020KJ023), Fundamental Research Program of Shanxi Province (Grant No. 202303021211324), Shanxi Scholarship Council of China (Grant No. 2020-133), Scientific and Technological Innovation Programs of Higher Education Institutions in Shanxi (Grant No. 2021L368, 2022L424), Postgraduate science and technology innovation project of Shanxi Normal University (Grant No. 2021XBY005).

Author contributions

ZB, LZ, HF, ZX, CW, ZL and MT performed the experiments. ZB, LZ and HZ analyzed the data, wrote the manuscript, and took part in discussions. YB and FF designed the experimental approach and supervised the project. All authors read and approved the final manuscript.

Availability of data and materials

The data that support the findings of this study are available from the corresponding authors upon reasonable request.

Declarations

Ethics approval and consent to participate

Animal experiments were performed under the permission of experimental animal ethics committee of Shanxi Datong University.

Consent for publication

All authors have seen the manuscript and approved the submission.

Competing interests

The authors declare that they have no competing interests.

Received: 19 March 2023 Accepted: 5 April 2023
Published online: 17 April 2023

References

Alijani H, Noori A, Faridi N, Bathaie SZ, Mousavi MF (2020) Aptamer-functionalized Fe_3O_4@MOF nanocarrier for targeted drug delivery and fluorescence imaging of the triple-negative MDA-MB-231 breast cancer cells. J Solid State Chem 292:121680

Arslan FB, Atar KO, Calis S (2021) Antibody-mediated drug delivery. Int J Pharm 596:120268

Chang X, Wu Q, Wu Y, Xi X, Cao J, Chu H, Liu Q, Li Y, Wu W, Fang X, Chen F (2022) Multifunctional Au modified Ti_3C_2-MXene for photothermal/enzyme dynamic/immune synergistic therapy. Nano Lett 22:8321–8330

Correa LB, Pinto SR, Alencar LMR, Missailidis S, Rosas EC, Henriques M, Santos-Oliveira R (2022) Nanoparticle conjugated with aptamer anti-MUC1/Y for inflammatory arthritis. Colloids Surf B Biointerfaces 211:112280

Du P, Yan J, Long S, Xiong H, Wen N, Cai S, Wang Y, Peng D, Liu Z, Liu Y (2020) Tumor microenvironment and NIR laser dual-responsive release of berberine 9-O-pyrazole alkyl derivative loaded in graphene oxide nanosheets for chemo-photothermal synergetic cancer therapy. J Mater Chem B 8:4046–4055

Gogotsi Y, Anasori B (2019) The rise of MXenes. ACS Nano 13:8491–8494

Han X, Huang J, Lin H, Wang Z, Li P, Chen Y (2018) 2D ultrathin MXene-based drug-delivery nanoplatform for synergistic photothermal ablation and chemotherapy of cancer. Adv Healthc Mater 7:1701394

He PP, Du X, Cheng Y, Gao Q, Liu C, Wang X, Wei Y, Yu Q, Guo W (2022) Thermal-responsive MXene-DNA hydrogel for near-infrared light triggered localized photothermal-chemo synergistic cancer therapy. Small 18:2200263

Huang H, Dong C, Feng W, Wang Y, Huang B, Chen Y (2022) Biomedical engineering of two-dimensional MXenes. Adv Drug Deliver Rev 184:114178

Khan H, Makwana V, Santos SND, Bonacossa de Almeida CE, Santos-Oliveira R, Missailidis S (2021) Development, characterization, and In Vivo evaluation of a novel aptamer (Anti-MUC1/Y) for breast cancer therapy. Pharmaceutics. 13:1239

Li GQ, Zhong XY, Wang XW, Gong F, Lei HL, Zhou YK, Li CF, Xiao ZD, Ren GX, Zhang L et al (2022) Titanium carbide nanosheets with defect structure for photothermal-enhanced sonodynamic therapy. Bioact Mater 8:409–419

Li L, Xu S, Yan H, Li X, Yazd HS, Li X, Huang T, Cui C, Jiang J, Tan W (2021) Nucleic acid aptamers for molecular diagnostics and therapeutics: advances and perspectives. Angew Chem Int Ed 60:2221–2231

Li M, Lu J, Luo K, Li Y, Chang K, Chen K, Zhou J, Rosen J, Hultman L, Eklund P et al (2019) Element replacement approach by reaction with lewis acidic molten salts to synthesize nanolaminated MAX phases and MXenes. J Am Chem Soc 141:4730–4737

Li Z, Zhang H, Han J, Chen Y, Lin H, Yang T (2018) Surface nanopore engineering of 2D MXenes for targeted and synergistic multitherapies of hepatocellular carcinoma. Adv Mater 30:1706981

Liang R, Li Y, Huo M, Lin H, Chen Y (2019) Triggering sequential catalytic fenton reaction on 2D MXenes for hyperthermia-augmented synergistic nanocatalytic cancer therapy. ACS Appl Mater Interfaces 11:42917–42931

Lin H, Wang X, Yu L, Chen Y, Shi J (2017) Two-dimensional ultrathin MXene ceramic nanosheets for photothermal conversion. Nano Lett 17:384–391

Liu C, Zhang T, Chen L, Chen Y (2020) The choice of anti-tumor strategies based on micromolecules or drug loading function of biomaterials. Cancer Lett 487:45–52

Liu G, Zou J, Tang Q, Yang X, Zhang Y, Zhang Q, Huang W, Chen P, Shao J, Dong X (2017) Surface modified Ti_3C_2 MXene nanosheets for tumor targeting photothermal/photodynamic/chemo synergistic therapy. ACS Appl Mater Interfaces 9:40077–40086

Liu K, Liao Y, Zhou Z, Zhang L, Jiang Y, Lu H, Xu T, Yang D, Gao Q, Li Z et al (2022b) Photothermal-triggered immunogenic nanotherapeutics for optimizing osteosarcoma therapy by synergizing innate and adaptive immunity. Biomaterials 282:121383

Liu M, Wang L, Lo Y, Shiu SC, Kinghorn AB, Tanner JA (2022a) Aptamer-enabled nanomaterials for therapeutics. Drug Target Imaging Cells 11:159

Liu Z, Xie L, Yan J, Liu PF, Wen HX, Liu HJ (2021) Folic acid-targeted MXene nanoparticles for doxorubicin loaded drug delivery. Aust J Chem 74:847–855

Lu BB, Hu SY, Wu D, Wu CY, Zhu ZY, Hu L, Zhang JH (2022) Ionic liquid exfoliated $Ti_3C_2T_x$ MXene nanosheets for photoacoustic imaging and synergistic photothermal/chemotherapy of cancer. J Mater Chem B 10:1226–1235

Naguib M, Kurtoglu M, Presser V, Lu J, Niu J, Heon M, Hultman L, Gogotsi Y, Barsoum MW (2011) Two-dimensional nanocrystals produced by exfoliation of Ti_3AlC_2. Adv Mater 23:4248–4253

Pan QS, Nie CP, Hu YL, Yi JT, Liu C, Zhang J, He MM, He MY, Chen TT, Chu X (2020) Aptamer-functionalized DNA origami for targeted codelivery of antisense oligonucleotides and doxorubicin to enhance therapy in drug-resistant cancer cells. ACS Appl Mater Interfaces 12:400–409

Roper DK, Ahn W, Hoepfner M (2007) Microscale heat transfer transduced by surface plasmon resonant gold nanoparticles. J Phys Chem C 111:3636–3641

Sargazi S, Er S, Mobashar A, Gelen SS, Rahdar A, Ebrahimi N, Hosseinikhah SM, Bilal M, Kyzas GZ (2022) Aptamer-conjugated carbon-based nanomaterials for cancer and bacteria theranostics: a review. Chem Biol Interact 361:109964

Tan Y, Li YY, Qu YX, Su YY, Peng YB, Zhao ZL, Fu T, Wang XQ, Tan WH (2021) Aptamer-peptide conjugates as targeted chemosensitizers for breast cancer treatment. ACS Appl Mater Interfaces 13:9436–9444

Tang W, Dong Z, Zhang R, Yi X, Yang K, Jin M, Yuan C, Xiao Z, Liu Z, Cheng L (2019) Multifunctional two-dimensional core-shell MXene@gold nanocomposites for enhanced photo-radio combined therapy in the second biological window. ACS Nano 13:284–294

VahidMohammadi A, Rosen J, Gogotsi Y (2021) The world of two-dimensional carbides and nitrides (MXenes). Science. 372:1581

Vandghanooni S, Barar J, Eskandani M, Omidi Y (2020) Aptamer-conjugated mesoporous silica nanoparticles for simultaneous imaging and therapy of cancer. TrAC, Trends Anal Chem 123:115759
Wu YZ, Xiong WF, Wang ZK, Wang Y, Sun KY, Song XR, Lv ZY, Xu W, Zhong W, Zou XP et al (2022) Self-assembled MXene-based Schottky-junction upon Transition metal oxide for regulated tumor microenvironment and enhanced CDT/PTT/MRI activated by NIR irradiation. Chem Eng J 427:131925
Xie S, Ai L, Cui C, Fu T, Cheng X, Qu F, Tan W (2021) Functional aptamer-embedded nanomaterials for diagnostics and therapeutics. ACS Appl Mater Interfaces 13:9542–9560
Xu YJ, Wang YW, An J, Sedgwick AC, Li M, Xie JL, Hu WB, Kang JL, Sen S, Steinbrueck A et al (2022) 2D-ultrathin MXene/DOX-jade platform for iron chelation chemo-photothermal therapy. Bioact Mater 14:76–85
Yang Y, Han Y, Sun Q, Cheng J, Yue C, Liu Y, Song J, Jin W, Ding X, de la Fuente JM et al (2021) Au-siRNA@ aptamer nanocages as a high-efficiency drug and gene delivery system for targeted lung cancer therapy. J Nanobiotechnol 19:54
Yathindranath V, Sun Z, Worden M, Donald LJ, Thliveris JA, Miller DW, Hegmann T (2013) One-pot synthesis of iron oxide nanoparticles with functional silane shells: a versatile general precursor for conjugations and biomedical applications. Langmuir 29:10850–10858
Yuhan J, Zhu LY, Zhu LJ, Huang KL, He XY, Xu WT (2022) Cell-specific aptamers as potential drugs in therapeutic applications: a review of current progress. J Control Release 346:405–420
Zhang M, Yang DY, Dong CH, Huang H, Feng GY, Chen QQ, Zheng YY, Tang HL, Chen Y, Jing XX (2022) Two-dimensional MXene-originated in situ nanosonosensitizer generation for augmented and synergistic sonodynamic tumor nanotherapy. ACS Nano 16:9938–9952
Zhu LJ, Yang JP, Ma Y, Zhu XY, Zhang C (2022) Aptamers entirely built from therapeutic nucleoside analogues for targeted cancer therapy. J Am Chem Soc 144:1493–1497

Publisher's Note